Research Square

Preprints are preliminary reports that have not undergone peer review.
They should not be considered conclusive, used to inform clinical practice,
or referenced by the media as validated information.

Thermodynamic Modeling and Waste Valorization for Sustainable Self-Glazed Ceramic Tiles Using Induction Furnace Slag

S Sadakat Sharif
Bangladesh University of Engineering and Technology
Rexona Khanom
Bangladesh Council of Scientific and Industrial Research (BCSIR)
Sazzad Ahmad
Chittagong University of Engineering and Technology
Bima Satritama
Swinburne University of Technology
M Akbar Rhamdhani
Swinburne University of Technology
Muzahidur Rahman Chowdhury
Bangladesh University of Engineering and Technology
Wahidur Rahman Sajal
Bangladesh University of Engineering and Technology
Muhammad Hasanuzzaman
Bangladesh University of Engineering and Technology
Fahmida Gulshan
fahmidagulshan@mme.buet.ac.bd

Bangladesh University of Engineering and Technology

Article

Keywords: Self-glazed tiles, IF slag, Waste glass, Thermodynamic modeling, FactSage

Posted Date: September 1st, 2026

DOI: https://doi.org/10.21203/rs.3.rs-10567762/v1

License: This work is licensed under a Creative Commons Attribution 4.0 International License.
Read Full License

Additional Declarations: No competing interests reported.

Thermodynamic Modeling and Waste Valorization for Sustainable Self-Glazed Ceramic Tiles Using Induction Furnace Slag

S Sadakat Sharif[1], Rexona Khanom[2*], Sazzad Ahmad[3], Bima Satritama[4], M Akbar Rhamdhani[4], Muzahidur Rahman Chowdhury[1], Wahidur Rahman Sajal[1], Muhammad Hasanuzzaman[1], Fahmida Gulshan[1*].

1. Bangladesh University of Engineering and Technology, Dhaka, 1000, Bangladesh
2. Bangladesh Council of Scientific and Industrial Research (BCSIR), Dhanmondi, Dhaka-1205, Bangladesh
3. Chittagong University of Engineering and Technology, Chattogram, 4349, Bangladesh
4. Swinburne University of Technology, Hawthorn, VIC 3122, Australia

ABSTRACT

The increasing demand for sustainable ceramic production has prompted research into alternative raw materials that minimize energy consumption, reduce reliance on natural resources, and utilize materials otherwise considered hazardous waste. This study explores the production of self-glazed ceramic tiles by incorporating Induction Furnace (IF) slag and waste glass as substitutes for conventional raw materials. A systematic compositional design was assessed using thermodynamic modeling, utilizing FactSage 8.2 thermochemical package, to reduce experimental workload and predict the role of IF slag in ceramic tile systems, followed by experimental validation to optimize vitrification, viscosity, and phase evolution. Results demonstrated that the presence of manganese and silica-rich IF slag significantly enhanced fluxing action, enabling complete vitrification at reduced firing temperatures by ~10%, as compared to without-slag tiles. Among the tested systems, the clay reduction strategy with 30 wt. % IF slag offered the most industrially viable performance, achieving excellent densification, minimal porosity (0.07%), high bulk density (3.95 g/cm^3), superior mechanical strength (64.3 MPa, modulus of rupture-MOR), and outstanding optical properties (translucency: 17.6%). These findings confirm that IF slag and waste glass can serve as effective raw material substitutes for sustainable ceramic tile production, reducing energy demand while valorizing metallurgical waste.

Keyword: Self-glazed tiles; IF slag; Waste glass; Thermodynamic modeling; FactSage.

**Corresponding author:* *Fahmida Gulshan; Present Address: Faculty Member of Materials and Metallurgical Engineering, Bangladesh University of Engineering and Technology, Dhaka-1000, Bangladesh. Phone +8801733892419;*
Email: fahmidagulshan@mme.buet.ac.bd

1. Introduction

The accelerating depletion of Earth's natural resources and the mounting environmental burden from industrial waste have underscored the urgent need for sustainable material alternatives and circular resource utilization. Among various industrial byproducts, steel slag, once considered an undesirable waste, has gained increasing attention for its potential in value-added applications across multiple sectors. The properties and composition of steel slag are strongly influenced by the steelmaking process used. Depending on the production route, various types of slag are produced, such as basic oxygen furnace (BOF) slag, electric arc furnace (EAF) slag, and induction furnace (IF) slag, each with distinct chemical characteristics. In general, steel slag is rich in calcium silicates, aluminosilicates, and iron oxides, and often contains alkali and alkaline earth elements that can serve as natural fluxing agents [1,2]. These steel slags can be used as raw materials in building construction and related materials [3,4].

Bangladesh's steel industry includes around 400 mills that produce approximately 4 million tonnes of steel each year, mostly using induction furnaces. This process generates a significant amount of slag, with an estimated 11 to 15 kilograms of IF slag produced for every ton of steel [5]. As a result, the country is estimated to produce about 60,0000 tonnes of slag annually, even though no official data is currently available [6]. Although IF slag has shown significant potential for reuse in various sectors due to its favorable chemical and mineralogical composition, its application in the ceramic industry remains largely underexplored. To date, the primary areas of IF slag utilization include concrete production, radiation shielding, marine infrastructure, antibacterial materials, and energy efficiency in steelmaking processes [7–13]. IF slag primarily consists of metal oxides, silicates, and aluminates and the major components include SiO_2, Al_2O_3, CaO, MgO and Fe_2O_3, with minor amounts of MnO, Cr_2O_3, P_2O_5, TiO_2, K_2O, and Na_2O [6,12,14]. Ceramic tiles are generally composed of aluminosilicate matrices, where SiO_2 and Al_2O_3 function as primary network-forming agents [15]. In addition, fluxing oxides such as Na_2O, K_2O, CaO, and MgO are crucial for lowering the vitrification temperature, enhancing liquid phase formation, and promoting densification during the firing process [16]. The presence of these fluxing components in IF slag suggests its promising role as a secondary raw material for ceramic applications, particularly in the development of self-glazed tiles, where surface vitrification is heavily influenced by the flux content. Based on this compatibility, it is reasonable to infer that IF slag holds significant potential for use in ceramic tile production. Its integration into structural ceramic products, such as self-glazed tiles, offers a sustainable solution for managing this hazardous industrial waste. This innovative reuse pathway not only contributes to waste valorization but also supports key industrial sectors by aligning with market trends focused on sustainable materials. Moreover, the substitution of IF slag for conventional raw materials could reduce reliance on natural resources and help lower firing temperatures, thereby decreasing overall energy consumption.

Similar to steel slag, waste glass has also gained attention for its potential reuse in construction and material applications, driven by environmental concerns and the growing emphasis on sustainable resource management [17]. Glass is one of the most widely used materials globally, but postconsumer glass often ends up in landfills due to contamination, color variation, and limited recycling infrastructure. In recent years, the construction industry, particularly the concrete sector, has emerged as a major avenue for waste glass utilization, offering a sustainable solution to reduce environmental impact while conserving raw materials and landfill space [18–20]. Waste glass functions effectively as a fluxing agent and sintering aid in

ceramic production, owing to its amorphous silica-rich composition. Its inclusion lowers the required sintering temperature, promotes densification, reduces porosity, and improves the mechanical integrity of the final product, even under reduced firing conditions [21–23]. Studies have shown that incorporating 10 to 30 percent glass waste can significantly enhance compressive and flexural strength, making it suitable for structural applications such as tiles, bricks, and blocks [21–24]. Furthermore, the addition of waste glass leads to decreased water absorption and increased density, resulting in ceramics with improved durability [21–24]. When used in combination with other industrial wastes, waste glass also contributes to the immobilization of heavy metals, facilitating the development of environmentally safe glass-ceramic materials [21–27]. While several studies have evaluated BOF and EAF slags in ceramics, the utilization of IF slag for self-glazed tiles remains largely unexplored, particularly in combination with waste glass[28–33] .

This study aims to evaluate the recycling potential of IF slag generated by the Bangladeshi steel industry in combination with discarded waste glass, with a particular focus on its suitability for self-glazed ceramic tile applications. The research promotes the environmentally responsible and sustainable reuse of IF slag and waste glass as alternative ceramic raw materials, contributing to both waste minimization and natural resource conservation. This study specifically investigates the effects of key process parameters on the performance of self-glazed ceramic tiles incorporating IF slag and waste glass using thermodynamic modeling and experimental investigation. These parameters include the optimal raw material ratio with the highest feasible incorporation of IF slag, the functional role of IF slag within the ceramic matrix, the most suitable firing temperature, the viscosity characteristics during sintering, and a comprehensive phase analysis of the final products. In addition, essential physical properties such as linear shrinkage, apparent porosity, water absorption, bulk density, modulus of rupture, and translucency will be systematically assessed to determine the overall performance and quality of the developed tiles.

2. Experimental Materials and Methodology

2.1 Raw Materials

IF steel slags were collected from a local steel plant in Bangladesh, while waste glass was obtained from a local glass industry. China clay and K-feldspar were procured separately from the local market. All raw materials were subjected to particle size analysis. IF slag and waste glass were crushed and ground prior to analysis. Laser particle size analysis using a Malvern Mastersizer 3000 showed D90 values of China clay: 55.7 μm, waste glass: 99.2 μm, K-feldspar: 247 μm, and IF slag: 35.9 μm.

2.2 Methodology

Chemical composition of raw materials (China clay, K-feldspar, waste glass and IF slag) was determined using X-ray fluorescence spectroscopy (XRF-1800, Shimadzu). Phase identification of IF slag and fired ceramic samples was conducted using X-ray diffraction (XRD, Rigaku SmartLab) with Cu Kα radiation (λ = 1.54059 Å) over a 2θ range of 10-80° at a scan rate of 0.16°/second. The surface morphology of the ceramic tiles was analyzed using a field emission scanning electron microscope (FESEM) (JEOL, JSM-7600F, Japan).

Physical and mechanical properties of the fired ceramic tiles were evaluated through multiple standardized tests. Linear shrinkage was measured according to ASTM C326-09 standard using equation (1).

$$\text{Linear Shrinkage, } L_S(\%) = \frac{L_p - L_f}{L_p} \times 100 \quad (1)$$

where L_p and L_f represent dry and fired lengths, respectively.

Water absorption, apparent porosity, and bulk density were determined using Archimedes' principle following ASTM C373-14 standard and using equation (2), (3) and (4).

$$\text{Water Absorption } (\%) = \frac{M_{sa} - M_{da}}{M_{da}} \times 100 \quad (2)$$

$$\text{Apparent porosity } (\%) = \frac{M_{sa} - M_{da}}{M_{sa} - M_{sw}} \times 100 \quad (3)$$

$$\text{Bulk Density } (\text{g/cm}^3) = \frac{M_{da}}{M_{sa} - M_{sw}} \quad (4)$$

where M_{da}, M_{sa}, and M_{sw} represent dry mass, saturated mass, and suspended saturated mass, respectively. Modulus of rupture (MOR) was measured using three-point bending test according to ASTM C1161-18 followed by equation (5).

$$\text{MOR (MPa)} = \frac{3 \times F \times L}{2 \times W \times D^2} \quad (5)$$

where F is maximum load (N), L is span length (mm), W is width (mm), and D is thickness (mm).

Translucency measurements of self-glazed tiles were performed at 85° reflection angle following ASTM D523 using a gloss meter (Multi Gloss 268 Plus, Konica Minolta).

2.3 Thermodynamic Modelling

FactSage 8.2 'Equilib' module was employed to predict the phase assemblages and liquid phase formation during the sintering of ceramic tile formulations at a temperature range of 900 to 1200 °C. Furthermore, the equilibrium phase diagrams were calculated using 'Phase Diagram' module. The phase diagram of SiO_2–Al_2O_3–MnO systems with addition of different minor oxides (K_2O, Na_2O, CaO, Fe_2O_3, TiO_2) were calculated based on compositional design. SiO_2, Al_2O_3, MnO were used as the three fixed axis of the phase diagram.

Sample compositions were input as their corresponding oxide constituents, derived from the chemical analysis of raw materials. The simulations utilized three integrated databases: FactPS (pure substances), FToxid (oxide solutions, slags, and glasses), and FTmisc (miscellaneous phases including spinels and complex ceramic compounds). The viscosity of the resulting liquid phases was analyzed using the Viscosity module in conjunction with the Melts database, providing critical insights into melt flow behavior and vitrification dynamics across the selected temperature range.

This thermodynamic modeling approach facilitated the prediction of several key parameters:

- Phase diagram for different compositions
- The proportion of liquid phase formation as a function of temperature
- Evolution of dominant crystalline phases
- Viscosity trends of the liquid phase during firing
- Optimal firing temperatures for each formulation
- Comparative vitrification behavior between different material systems

All calculations were carried out under oxidizing atmospheric conditions (air) at standard atmospheric pressure (1 atm), simulating realistic industrial ceramic firing environments. The thermodynamic predictions served as a foundational tool for guiding experimental validation and optimizing the incorporation of IF slag into ceramic tile compositions.

2.4 Sample Preparation

2.4.1 Compositional Design

Eight compositions with varying ratios of IF steel slag were systematically designed for thermodynamic simulation analysis (Table 1). The design followed a methodical approach involving two distinct formulation strategies:

System 1 (Samples 2–5): Using Sample 1 as the baseline, this system was designed by fixing the waste glass and K-feldspar content at 30% each, while varying the IF slag from 0% to 40% and proportionally reducing China clay from 40% to 0%. This strategy aimed to examine the effect of clay reduction on vitrification behavior while keeping the overall flux content constant.

System 2 (Samples 6–8): Also referencing Sample 1, this configuration maintained constant levels of waste glass (30%) and China clay (40%), while decreasing K-feldspar from 20% to 0% and increasing IF slag from 10% to 30%. The goal was to evaluate the feasibility of replacing traditional alkali fluxes with metallurgical waste.

The complete compositional matrix of these formulations is presented in Table 1, representing a comprehensive experimental design for optimizing IF slag utilization in ceramic tile applications.

Table 1: Composition of base mixture (in wt. %)

	K- Feldspar	Waste glass	China clay	IF slag
Sample 1	30	30	40	0
Sample 2	30	30	30	10
Sample 3	30	30	20	20
Sample 4	30	30	10	30
Sample 5	30	30	0	40
Sample 6	20	30	40	10
Sample 7	10	30	40	20
Sample 8	0	30	40	30

2.4.2 Physical Sample Preparation and Processing

For experimental validation, 1 kg batches of each composition were prepared by accurately weighing the constituent raw materials according to the designed formulations. The dry ingredients were subjected to wet ball milling with 600 mL distilled water for 12 hours to ensure homogeneous mixing and particle size reduction. The resulting slurry was subsequently dried at ambient temperature (25 °C) for two weeks to achieve complete moisture removal and prevent cracking during the drying process. The dried mixture was pulverized using a crushing mortar to break up any agglomerated particles and ensure uniform powder characteristics. Test specimens were prepared by weighing 24 g portions of the pulverized mixture and adjusting the moisture content to approximately 7 wt. % through controlled water spraying to achieve optimal pressing conditions. Green tiles with dimensions of 90 × 20 × 8 mm were formed using a hydraulic press operating at 8 tonnes pressure. The pressed green bodies were dried at 110 °C for 24 hours in a laboratory oven to eliminate residual moisture and prevent cracking during subsequent firing. The sintering process was conducted in a laboratory box furnace with temperature profiles optimized based on compositional requirements: Eight self-glazed tiles of Sample 1 were fired at temperature intervals across 1025–1150 °C to determine its vitrification pathway. By contrast, Samples 2–4 were fired as four tiles within the reduced range of 1040–1075 °C, reflecting the stronger fluxing role of IF slag. All compositions were subjected to a soaking time of 1 hour at peak temperature to ensure complete vitrification and development of the desired microstructure for self-glazed ceramic tiles.

3. Results and Discussion

3.1 Characterization of Raw Materials

The chemical compositions of the raw materials used in this study are presented in Table 2 (in wt. %), based on analysis conducted using X-ray fluorescence. K-feldspar was predominantly composed of SiO_2, Al_2O_3, and K_2O, with minor amounts of Na_2O and Fe_2O_3. Glass waste exhibited an exceptionally high silica content (96.24%) and contained small quantities of Al_2O_3, Na_2O, CaO, Fe_2O_3 and MgO. China clay was rich in SiO_2 (64.57%) and Al_2O_3 (28.35%), along with trace amounts of other oxides. IF slag characterized by a high concentration of MnO, SiO_2, Al_2O_3 and Fe_2O_3. It also contained notable amounts of CaO (3.78%), MgO (1.40%), TiO_2 (3.07%), and minor oxides such as Cr_2O_3, SO_3, BaO, and ZrO_2.

Table 2: Chemical Composition of Raw materials (in wt. %)

Element	K-Feldspar	Waste glass	China clay	IF slag
SiO_2	66.68	96.24	64.57	46.89
Al_2O_3	12.51	0.99	28.35	7.45
K_2O	17.253	0.13	1.05	0.59
Na_2O	2.78	0.76	0	0.46
CaO	-	0.697	0.38	3.78
Fe_2O_3	0.193	0.304	3.37	6.01
MgO	-	0.885	0.27	1.402
MnO	-	-	-	29.36
TiO_2	-	-	1.8	3.072
SO_3	-	-	-	0.11
BaO	-	-	-	0.56

P_2O_5	-	-	0.145	-
ZrO_2	-	-	0.09	0.03
Cr_2O_3	-	-	-	0.185

The XRD pattern of the IF slag sample reveals a complex crystalline structure dominated by quartz (SiO_2) and pyrolusite (MnO_2) phases, indicating significant silica content and manganese oxidation during the steel refining process (Figure 1). Although MnO_2 is observed at room temperature, it undergoes thermal decomposition to MnO above ~1000 °C. Since MnO is the stable form under ceramic firing conditions, it was considered in both the XRF quantification and the thermodynamic simulations. Other phases identified include spinel ($MgAl_2O_4$), which reflects the presence of magnesium and aluminum oxides in the slag composition, along with iron oxide phases comprising both hematite (Fe_2O_3) and magnetite (Fe_3O_4), demonstrating the varied oxidation states of iron present in the material. The sharp, high-intensity quartz peaks suggest extensive crystallization of the silicate matrix during cooling, whereas the presence of pyrolusite signifies oxidation of manganese-bearing phases under the oxidizing conditions of the steelmaking process.

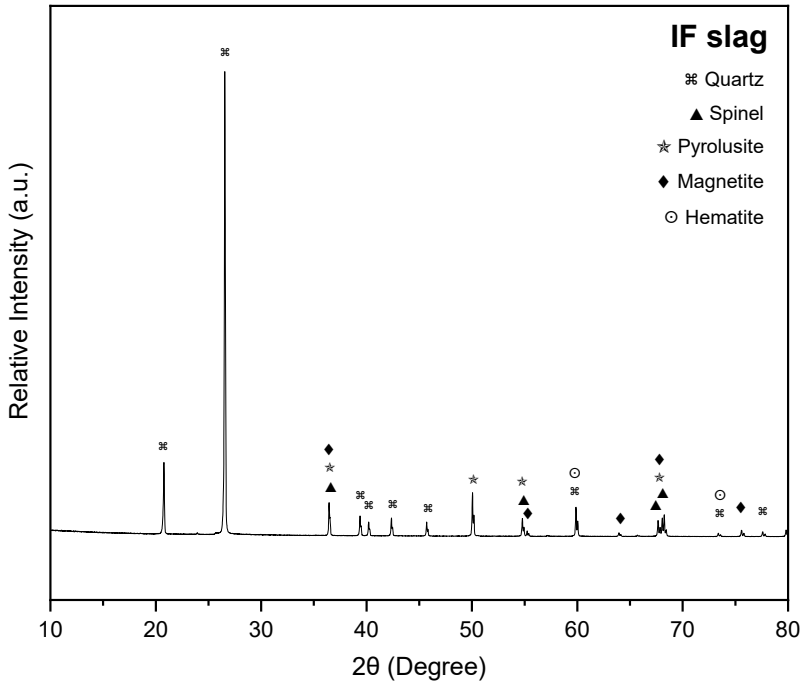


Figure 1: X-ray diffraction pattern of IF slag showing the identified crystalline phases

3.2 Thermodynamics Analysis of Equilibrium Products at Different Temperatures

The Table 3 presents the oxide compositions (in wt. %) of 8 simulated ceramic formulations prepared for input into FactSage thermodynamic calculations. The compositional data reflect the systematic variation approach employed in this study. Sample 1 mainly contains SiO_2 and Al_2O_3, serving as the control. System 1 (Samples 2–5) shows progressive reduction in SiO_2 (73.06 to 67.78%) and Al_2O_3 (13.32 to 7.05%) with corresponding increases in MnO (2.94 to 11.77%), demonstrating the clay reduction strategy. System 2 (Samples 6–8) exhibits

decreasing K_2O content (3.97 to 0.64%) with increasing MnO (2.94 to 8.81%), reflecting feldspar substitution with IF slag.

Table 3: Chemical composition of simulated final samples

Element	Sample							
	1	**2**	**3**	**4**	**5**	**6**	**7**	**8**
SiO_2	74.83	73.06	71.30	69.54	67.78	72.81	70.79	68.78
Al_2O_3	15.42	13.32	11.23	9.14	7.05	14.90	14.39	13.87
K_2O	5.64	5.60	5.55	5.51	5.46	3.97	2.30	0.64
Na_2O	1.06	1.11	1.16	1.20	1.25	0.83	0.60	0.37
CaO	0.36	0.70	1.04	1.38	1.72	0.74	1.12	1.50
Fe_2O_3	1.50	1.76	2.03	2.29	2.56	2.08	2.66	3.24
MgO	0.37	0.49	0.60	0.71	0.83	0.51	0.65	0.79
MnO	0.00	2.94	5.88	8.83	11.77	2.94	5.88	8.81
TiO_2	0.72	0.85	0.98	1.10	1.23	1.03	1.34	1.64
SO_3	0.00	0.01	0.02	0.03	0.04	0.01	0.02	0.03
BaO	0.00	0.06	0.11	0.17	0.22	0.06	0.11	0.17
P_2O_5	0.06	0.04	0.03	0.01	0.00	0.06	0.06	0.06
ZrO_2	0.04	0.03	0.02	0.02	0.01	0.04	0.04	0.05
Cr_2O_3	0.00	0.02	0.04	0.06	0.07	0.02	0.04	0.06

The phase relations of the SiO_2–Al_2O_3–MnO systems with minor fluxing oxides (K_2O, Na_2O, CaO, Fe_2O_3, TiO_2) were calculated using the Phase Diagram module of FactSage 8.2 (Figure 2 and Figure 3). These diagrams enabled evaluation of vitrification pathways and the influence of IF slag additions on the melting behavior of ceramic compositions. The calculated liquid stability fields appeared within a consistent temperature range of ~1079–1095 °C across all samples, indicating that while the onset of vitrification depends on composition, it is reproducible and thermodynamically accessible under practical firing conditions.

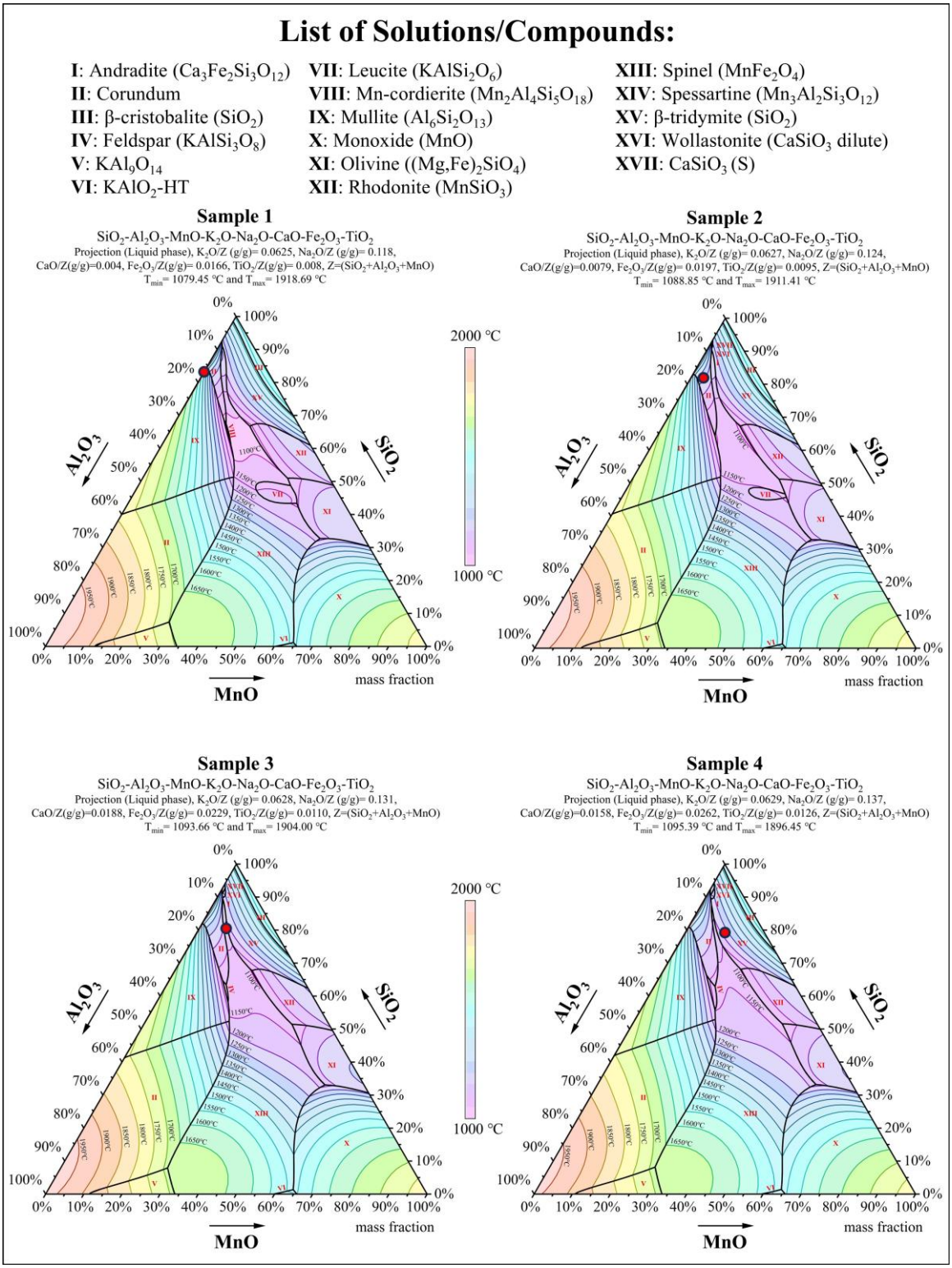


Figure 2: Pseudo-ternary SiO_2–Al_2O_3–MnO phase diagrams (Sample 1 to Sample 4)

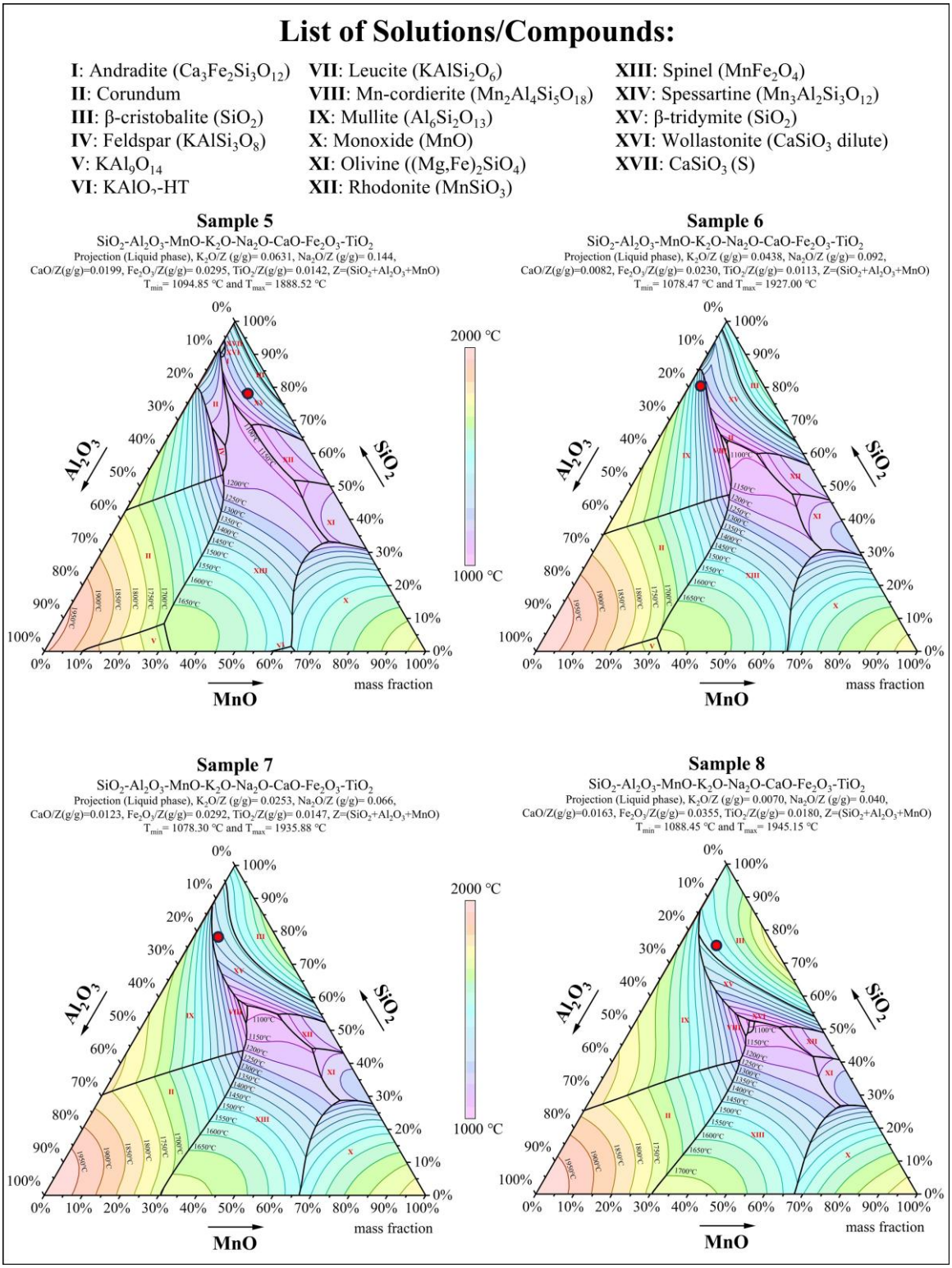


Figure 3: Pseudo-ternary SiO_2–Al_2O_3–MnO phase diagrams (Sample 5 to Sample 8)

The Figure 2 shows the positions of the compositions in the SiO_2–Al_2O_3–MnO ternary. Sample 1 falls within the mullite field along the ~1400 °C isotherm and, on cooling, moves toward the corundum–Mn-cordierite–mullite–liquid phase junction. Sample 2, in contrast, is initially located in the corundum region near the 1300 °C isotherm and, upon cooling, reaches the corundum–mullite–spinel–liquid phase junction at 1096.9 °C. This reflects a clear shift from mullite to corundum stability with the first addition of IF slag. Sample 3 is positioned on the corundum phase boundary at the ~1250 °C isotherm and approaches the feldspar–corundum–mullite–liquid phase junction at 1125.6 °C. With further IF slag addition (Samples 4 and 5), the compositions shift into the tridymite field. On cooling, they intersect the rhodonite–tridymite–spinel–liquid phase junction, corresponding to the lowest liquid-onset points at 1095.4 °C (Sample 4) and 1094.8 °C (Sample 5). However, Sample 5 lies in a higher-temperature zone (~1300 °C) compared to Sample 4 (~1200 °C), requiring more heat despite similar compositional trends.

In contrast, Sample 6 (Figure 3) remains in the mullite region but cools toward the Mn-cordierite–mullite–tridymite–liquid phase junction at ~1099.4 °C. Sample 7 lies in the tridymite field at the ~1400 °C isotherm and finishes at the same junction as Sample 6, with a liquid-onset of 1112.8 °C. Sample 8 is situated in the cristobalite field along the ~1500 °C isotherm and does not intersect a eutectic point upon cooling, confirming its substantially higher thermal requirement compared to System 1.

Overall, these results confirm that System 1, and especially Sample 4, can be processed at lower firing temperatures. This makes it the most favorable pathway for achieving vitrification.

Table 4 represents phase notation and chemical formula of equilibrium products which are calculated from 'equilib' simulation result.

Table 4: Phase notation and chemical formula of equilibrium products from Simulation

Phase Notation	**Chemical Formula**	**Phase Notation**	**Chemical Formula**
Quartz (solid)	SiO_2	Mullite	$3Al_2O_3.2SiO_2$
Mn-substituted cordierite (solid)	$Mn_2Al_4Si_5O_{18}$	Mn-rich garnet (solid)	$Mn_3Al_2Si_3O_{12}$
Cordierite	$Mg_2Al_4Si_5O_{18}$	Feldspar	$NaAlSi_3O_8$; $KAlSi_3O_8$; $CaAl_2Si_2O_8$
Hematite	Fe_2O_3	Spinel	$MnFe_2O_4$
Rutile	TiO_2	Enstatite	$MgSiO_3$
Rhodonite	$MnSiO_3$	Wollastonite	$CaSiO_3$
Liquid Phase	An amorphous and glassy liquid phase, mixture of different oxides		

The phase evolution trends for Samples 1–5 are shown in Figure 4, whereas Figure 5 depicts the results for Samples 6–8. Together, these diagrams emphasize how systematic compositional changes affect melting pathways and firing windows.

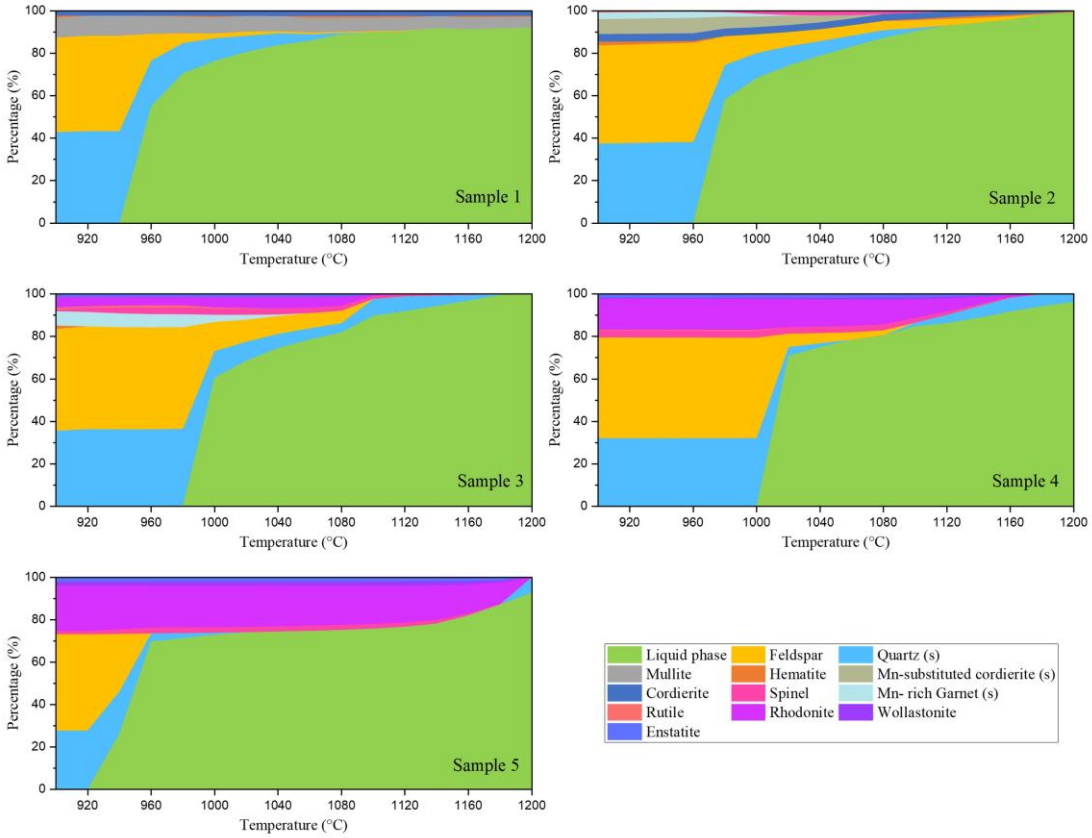


Figure 4: Phase equilibrium diagram for Sample 1 to sample 5

The thermodynamic analysis revealed that System 1 demonstrated superior vitrification performance through strategic clay reduction and IF slag incorporation (shown in Figure 4). Sample 2 achieved optimal liquid phase formation of 87.23% at 1080 °C, while ultimately reaching 99.27% at 1200 °C, representing the most efficient vitrification pathway among all tested compositions. Notably, while our optimized composition exceeded 87% liquid formation at 1080 °C, experimental studies in the literature typically report glass phase fractions of ~65% under similar firing conditions [34], underscoring the enhanced fluxing efficiency of IF slag in our system. Progressive IF slag incorporation systematically reduced quartz content from 42.44% (Sample 1) to 26.81% (Sample 5) at 900 °C, reflecting enhanced fluxing behavior attributed to MnO, CaO, and MgO in the slag composition. Diagnostic intermediate phases characteristic of Mn-bearing systems appeared exclusively in slag-containing compositions, with Sample 2 showing the most controlled Mn-rich garnet evolution from 3.04% at 900 °C to complete dissolution by 1040 °C, enabling gradual flux release during vitrification. Higher slag contents (Samples 3–5) promoted pyroxenoid phase formation including rhodonite, wollastonite, and enstatite, with Sample 5 exhibiting the highest rhodonite content (20.70% at 900 °C), though this persistence throughout the temperature range suggested incomplete integration and reduced vitrification efficiency (73.29% liquid at 1080 °C).

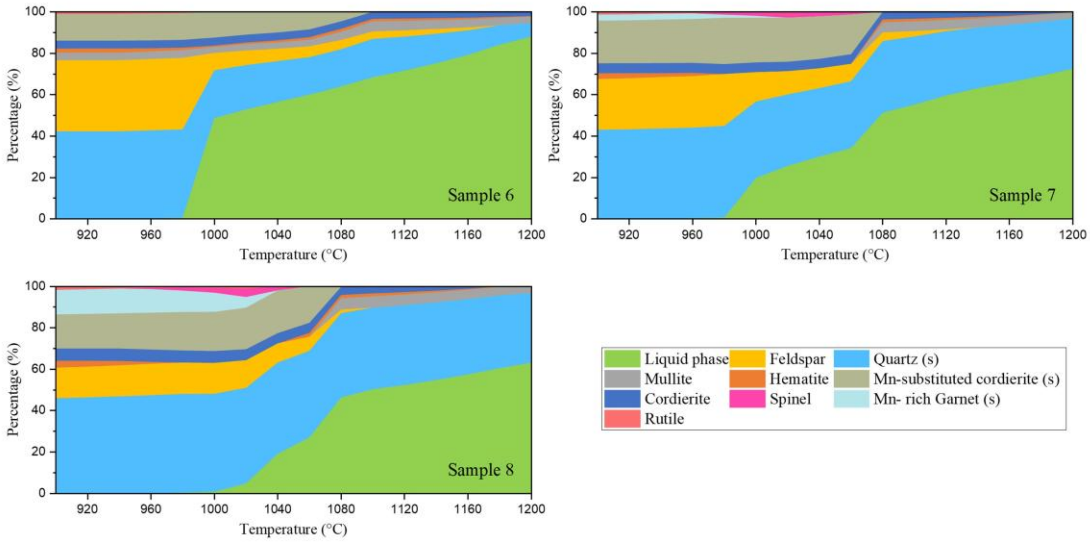


Figure 5: Phase equilibrium diagram for Sample 6 to sample 8

System 2 exhibited markedly inferior vitrification efficiency, requiring significantly higher temperatures for adequate melting compared to System 1. Sample 6 achieved only 87.96% liquid phase at 1200 °C, while Sample 8 demonstrated the best performance within this system at 96.80% liquid phase at 1200 °C, both substantially lower than System 1's performance. The delayed vitrification onset, beginning at 960 °C for most samples compared to earlier initiation in System 1, reflected reduced fluxing effectiveness when K-feldspar replaced clay components. Persistent formation of Mn-substituted cordierite (12.89–20.55% at 900 °C across Samples 6–8) created refractory networks that restricted vitrification throughout the temperature range. Despite Sample 8's high initial Mn-rich garnet content (11.80% at 900 °C), liquid phase formation remained severely limited to only 63.16% at 1200 °C, with substantial mullite development (5.49% at 1080 °C) occurring at economically unviable firing conditions for ceramic tile manufacturing.

Temperature-dependent phase evolution revealed distinct behavioral patterns across the two formulation strategies, with optimal performance occurring through different mechanisms. System 1 achieved efficiency through controlled intermediate phase dissolution and moderate slag incorporation, more particularly, Sample 2's balanced composition provided the widest processing window and most predictable vitrification. On the other hand, System 2's reliance on K-feldspar replacement consistently produced refractory phase assemblages that hindered liquid formation, making it unsuitable for industrial applications despite some samples showing reasonable performance at elevated temperatures. The formation and dissolution patterns of Mn-rich garnet phases emerged as critical indicators of vitrification efficiency across all systems, with controlled dissolution timing directly correlating with optimal liquid phase development.

While Sample 2 demonstrated superior laboratory vitrification performance, Sample 4 presents compelling advantages for industrial ceramic tile production. Sample 4 achieved substantial liquid phase formation (79.37% at 1080 °C) with delayed but controlled vitrification onset beginning at 1020 °C (69.38%), providing better process control and reducing over-firing risks

during large-scale manufacturing. The persistence of rhodonite phases in Sample 4 offers potential benefits for thermal shock resistance and mechanical properties, while its gradual vitrification curve (from 69.38% at 1020 °C to 96.32% at 1200 °C) provides a wider firing window crucial for maintaining consistent quality in industrial production. Considering the dual objectives of lowering firing temperature, maximizing waste utilization, and ensuring reliable industrial processing, System 1 with Sample 4 formulation represents the optimal balance between performance, economic viability, and processing requirements for sustainable ceramic tile production.

3.3 Calculation of Viscosity

Viscosity is a key factor in ceramic tile sintering, as it directly affects densification, microstructure development, stain resistance, and dimensional stability. Inadequate viscosity control can lead to defects: high viscosity impedes densification and promotes irregular porosity, while low viscosity increases the risk of pyroplastic deformation during firing [35]. During sintering, ceramics can be treated as linear viscous materials, with viscosity generally decreasing as temperature increases. However, densification and grain growth can lead to viscosity increases [36]. Thermodynamic simulations using software like FactSage can help optimize formulations and firing temperatures when incorporating waste glass [37]. Using the FactSage Viscosity module, the melt viscosity of all compositions was estimated across the firing temperature range. Figure 6 illustrates the viscosity-temperature curves at selected temperatures (900 °C to 1200 °C). Results are expressed in logarithmic scale (log (Pa.s)).

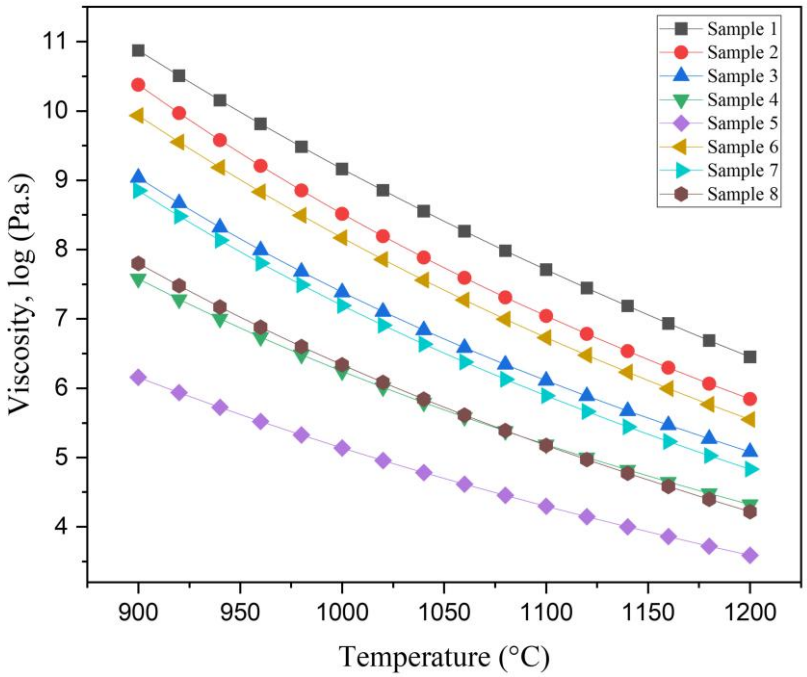


Figure 6: Viscosity of simulated ceramic tiles incorporated with IF slag, with different temperatures

The viscosity of the control composition (Sample 1) decreased from 10.87 (log (Pa.s)) at 900 °C to 6.45 at 1200 °C, indicating sluggish melt dynamics and delayed vitrification compared

to slag-containing formulations. In contrast, System 1 (Samples 2–5, clay-reduction with IF slag) showed a systematic reduction in viscosity with progressive slag addition. For example, Sample 2 dropped from 10.38 to 5.84 (≈ 7.31 at 1080 °C), Sample 3 from 9.04 to 5.08, and Sample 5 from 6.16 to 3.59. These marked decreases reflect enhanced fluxing action, producing highly fluid melts at elevated temperatures and enabling earlier liquid-phase formation within a broadened firing window.

System 2 (Samples 6–8, feldspar substitution with IF slag) exhibited intermediate viscosity profiles. Although values declined steadily with temperature, they remained consistently higher than those of slag-rich mixes in System 1. Sample 6 decreased from 9.93 at 900 °C to 5.55 at 1200 °C (≈ 7.00 at 1080 °C), Sample 7 from 8.85 to 4.83 (≈ 6.13 at 1080 °C), and Sample 8 from 7.80 to 4.22 (≈ 5.39 at 1080 °C). These results highlight that feldspar substitution requires greater thermal input to achieve melt fluidity comparable to clay-reduced formulations.

Overall, the comparison demonstrates that System 1 compositions provide the most effective viscosity reduction, supporting efficient sintering and liquid-phase development within the practical firing window of 1040–1080 °C. The exponential reduction in viscosity with temperature aligns with typical silicate melt behavior [38]. Maintaining viscosity within an optimal range allows ceramic tiles to develop improved microstructures and reduced porosity, while preserving dimensional stability during firing [35].

3.4 System Selection and Temperature Optimization

Based on the thermodynamic analysis, Samples 1–4 were selected for experimental production on the basis of their phase diagram trends, phase percentage calculations, superior vitrification performance, and favorable viscosity characteristics. In contrast, System 2 showed markedly lower vitrification efficiency and required significantly higher firing temperatures. Sample 5 was excluded because its clay-free composition resulted in poor plasticity, making shaping and forming impractical.

Sample 1, the control without IF slag, was fired across a wide temperature range (1025–1150 °C) to establish baseline vitrification behavior. Modeling indicated incomplete vitrification at 1040–1075 °C (8 self-glazed tiles), necessitating higher firing conditions to achieve sufficient liquid-phase formation. In contrast, Samples 2–4, with progressive IF slag additions (10%, 20%, and 30%), exhibited enhanced fluxing action from MnO, CaO, and MgO, enabling complete vitrification within the reduced firing window of 1040–1075 °C (4 self-glazed tiles).

Notably, Samples 3 and 4 showed signs of over-vitrification at 1075 °C, confirming that IF slag incorporation effectively lowered the optimal firing temperature while preserving excellent ceramic properties. These results align with the study objective of reducing energy consumption through lower firing temperatures while maximizing industrial waste utilization.

3.5 Experimental Investigations

3.5.1 Characterization of Experimental Samples

XRD analysis of Sample 1 reveals quartz as the predominant phase with mullite as a secondary phase throughout 1050–1150 °C (Figure 7). The persistence of both phases reflects limited fluxing capacity without slag incorporation, requiring higher temperatures for vitrification compared to slag-containing compositions [39]. Sample 2 shows reduced quartz intensity and

complete mullite elimination within 1040–1075 °C, indicating enhanced fluxing from MnO, CaO, and MgO in the slag [40]. Feldspar phases dissolve progressively from 1040 °C to 1075 °C, while cordierite appears initially then reduces with temperature. Spinel phases contribute to optimal vitrification efficiency at this moderate temperature range [41]. Sample 3 exhibits further quartz reduction and continued mullite absence within 1040–1075 °C. Pyroxenoid phases emerge, particularly rhodonite and wollastonite, which undergo systematic transformation contributing to controlled liquid phase development with slightly reduced efficiency compared to Sample 2. Sample 4 maintains quartz dominance with reduced intensity throughout 1040–1075 °C. The prominent rhodonite phase persists across the entire temperature range, indicating incomplete integration during vitrification. This controlled rhodonite dissolution provides a wider firing window, making Sample 4 optimal for industrial ceramic tile production despite moderate vitrification efficiency [42].

The systematic XRD analysis across Samples 1–4 reveals a clear progression in phase evolution with increasing IF slag content. The elimination of mullite phases beginning with Sample 2, the progressive reduction in quartz intensity, and the emergence of Mn-rich pyroxenoid phases (particularly rhodonite in Sample 4) directly correlate with the thermodynamic predictions. FactSage simulations had forecasted early mullite suppression, gradual quartz dissolution, and the appearance of Mn-bearing intermediate phases as key indicators of slag-driven vitrification. The experimental XRD results validate these predictions, confirming that modeling provided accurate guidance for composition selection and firing range optimization. The crystallographic evidence supports the conclusion that while Sample 2 demonstrates superior vitrification efficiency, Sample 4's unique phase assemblage, characterized by controlled rhodonite formation and gradual phase dissolution, offers optimal balance for industrial ceramic tile manufacturing through enhanced process control and wider firing windows.

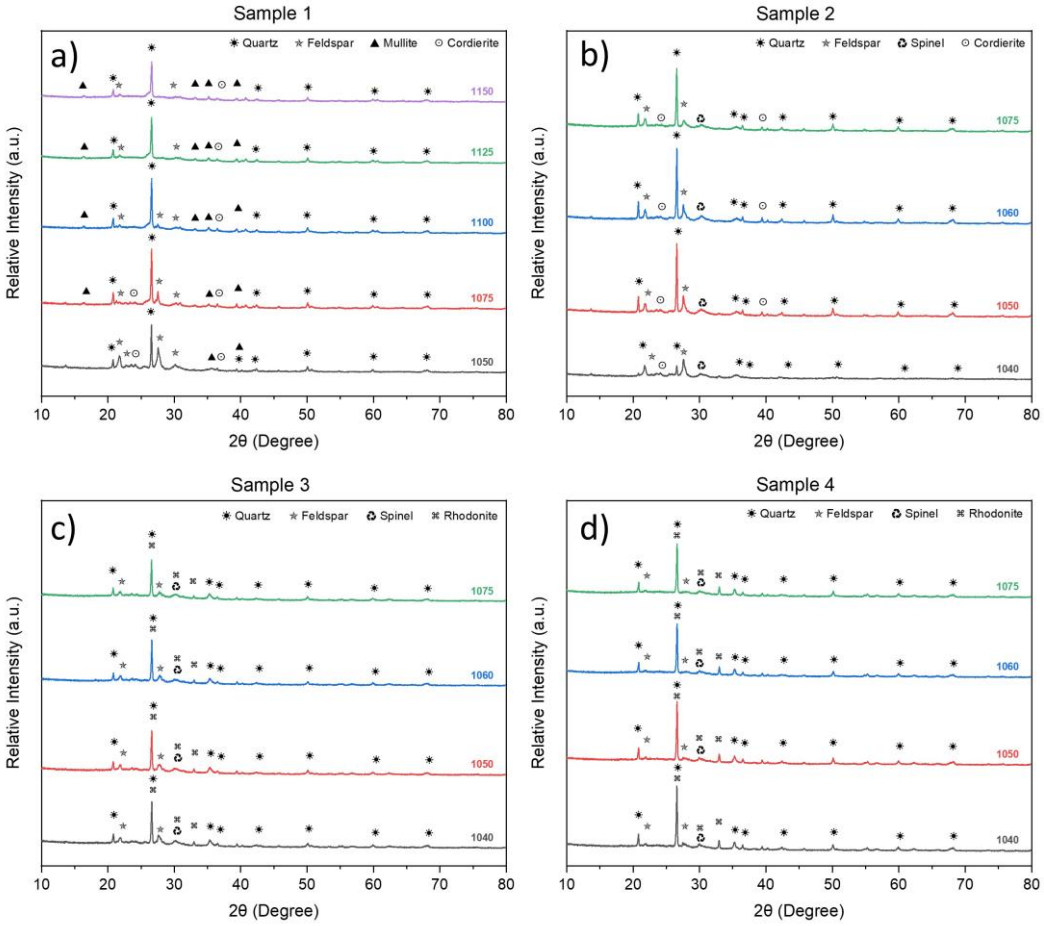


Figure 7: XRD analysis of self-glazed ceramic tile samples (Samples 1–4)

3.5.2 Physical and Microstructural Properties

The physical properties of ceramic tiles, including linear shrinkage, water absorption, apparent porosity, and bulk density, are interconnected parameters that provide comprehensive insights into sintering behavior, densification mechanisms, and microstructural evolution [43]. These properties are collectively influenced by raw material composition, firing temperature, and the presence of fluxing agents such as IF slag. Figure 8 depicts the Linear Shrinkage, Water Absorption, Apparent Porosity and Bulk Density Test result.

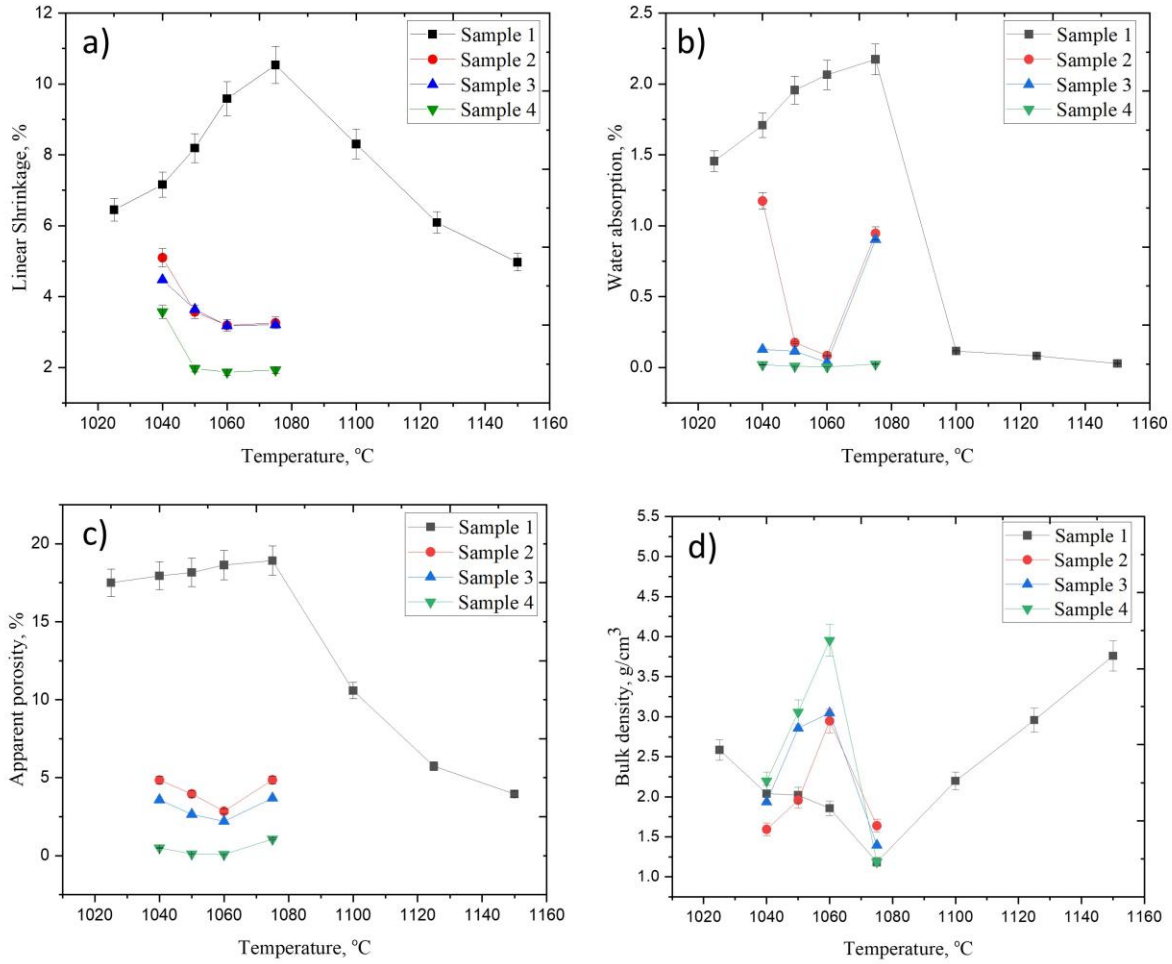


Figure 8: Linear Shrinkage (a), Water Absorption (b), Apparent Porosity (c) and Bulk Density (d) test result

Linear shrinkage is a critical parameter that reflects the dimensional changes occurring during the sintering process (Figure 8(a)). For the Sample 1, linear shrinkage exhibited a characteristic two-stage behavior: progressive increase up to 1075 °C (10.54%), followed by a significant reduction to 4.97% at 1150 °C. This pattern corresponds to the transition from initial particle rearrangement and neck formation to advanced densification with pore closure and glassy phase formation. The incorporation of IF slag fundamentally altered this sintering behavior. All slag-containing compositions demonstrated enhanced dimensional stability, with shrinkage values decreasing consistently up to 1060 °C, reaching minimum values of 1.87% for the Sample 4. This improvement is attributed to the formation of stable crystalline phases and early onset of vitrification facilitated by the fluxing action of slag components [44]. Shrinkage increased slightly beyond 1060 °C due to the onset of overheating, recrystallization, and thermal stress relaxation within the ceramic body.

Water absorption and apparent porosity measurements (Figure 8(b), Figure 8(c)) provide complementary information about the pore structure and permeability of the sintered tiles. The control sample exhibited increasing water absorption up to 1075 °C (2.17%) and apparent porosity up to 18.92%, indicating incomplete densification and high interconnected porosity.

At 1150 °C, both parameters decreased dramatically (water absorption: 0.028%, apparent porosity: 3.95%) due to the formation of a viscous liquid phase from feldspar and silica components, which penetrates and seals pores through capillary action and surface tension effects. The introduction of IF slag resulted in substantially improved performance across all compositions. Water absorption decreased consistently with temperature up to 1060 °C, reaching exceptionally low values of 0.0045% for Sample 4, while apparent porosity reduced to 0.074%. This superior performance is attributed to enhanced densification kinetics, reduced linear shrinkage, and the presence of MnO and other transition metal oxides that promote earlier vitrification and more effective pore closure [45].

Figure 9 presents SEM micrographs of the surface microstructure of ceramic tiles fired at their respective optimal temperatures. The control sample without IF slag (Sample 1, 1150 °C) exhibits a heterogeneous microstructure with residual pores and incomplete glass phase continuity, indicating delayed vitrification despite high firing temperature.

In contrast, slag-containing samples display a markedly denser and more uniform microstructure. Samples with 10–20 wt.% IF slag fired at 1060 °C shows a continuous glassy matrix with predominantly closed and rounded pores, reflecting enhanced melt formation and effective viscous flow during firing. The smooth pore boundaries and reduced pore connectivity indicate improved densification and self-glazing behavior. Increasing IF slag content promotes melt homogenization and pore rounding due to the fluxing action of MnO, CaO, and MgO present in the slag. However, localized pore enlargement and surface irregularities observed at higher slag contents are consistent with over-vitrification tendencies at elevated liquid fractions. Overall, the SEM observations corroborate the thermodynamic predictions and experimental results, confirming that controlled IF slag incorporation enhances vitrification while excessive liquid formation may induce bloating-related defects.

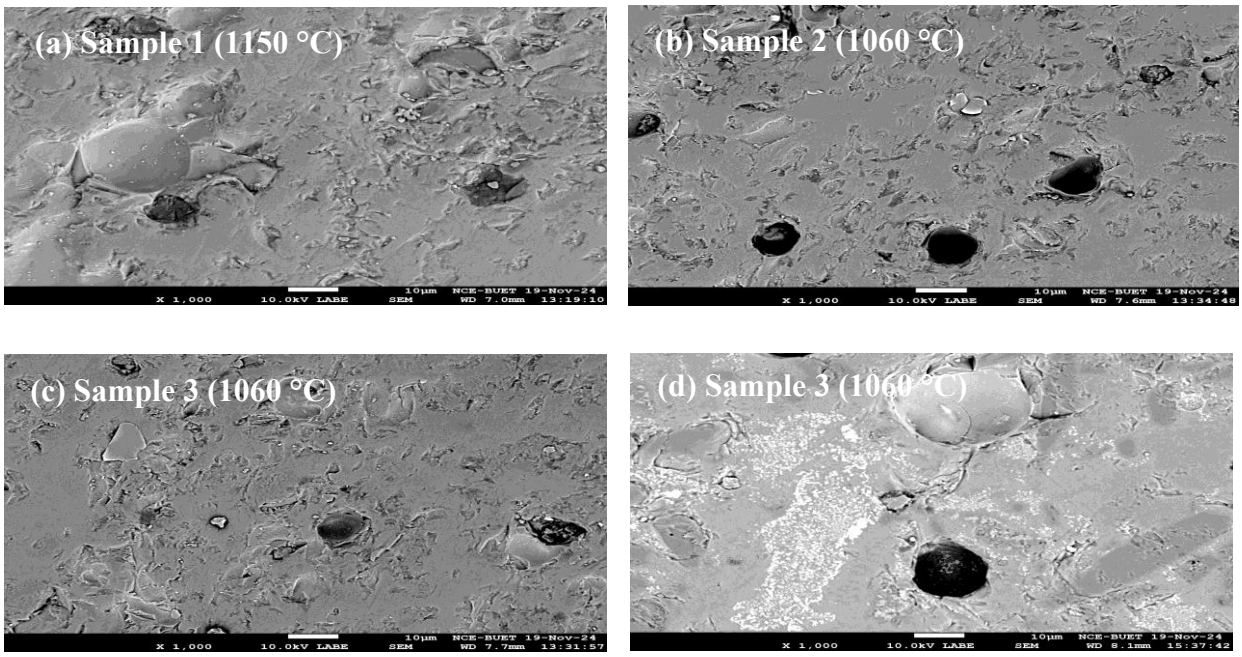


Figure 9: SEM micrographs of ceramic tile surfaces fired at their respective optimal temperatures.

Bulk density measurements (Figure 8(d)) provide direct quantitative evidence of densification effectiveness and microstructural compaction. The control sample showed decreasing density up to 1075 °C, followed by substantial improvement to 3.76 g/cm³ at 1150 °C, consistent with the completion of sintering processes and elimination of porosity. IF slag incorporation resulted in progressive density increases up to 1060 °C, with Sample 4 achieving 3.95 g/cm³. This enhancement reflects improved particle packing, higher cross-sectional density, and more efficient sintering kinetics facilitated by the fluxing action of slag components. The correlation between increased bulk density and reduced porosity/water absorption confirms the effectiveness of slag addition in promoting comprehensive densification [45,46].

Above the optimal firing temperature of 1060 °C, all slag-containing samples (Sample 2–Sample 4) exhibited deterioration in physical properties, including increased water absorption, apparent porosity, and reduced bulk density. This degradation is attributed to overheating-induced microstructural changes, including recrystallization, potential microcrack formation, grain growth, and stress relaxation phenomena. At excessive firing temperatures, the excessively low viscosity of the melt, combined with surface tension effects, promotes bloating and irregular glaze flow, thereby reducing the effectiveness of the self-glazing mechanism.

3.5.3 Mechanical Strength and Optical Properties

The mechanical strength and optical characteristics of ceramic tiles are crucial parameters that determine their suitability for specific applications and aesthetic appeal. Modulus of rupture (MOR) provides insights into mechanical integrity, while translucency measurements reveal surface vitrification and self-glazing effectiveness [47]. Figure 10 depicts the MOR and translucency results. Tiles characterized by elevated MOR are less susceptible to cracking or breaking when subjected to bending forces. According to ASTM C1505, minimum MOR values of 25 MPa and 35 MPa are required for wall and floor tiles, respectively. The MOR evolution with temperature and composition (Figure 10(a)) demonstrates the critical relationship between microstructural development and mechanical performance.

The control sample (Sample 1, with no slag addition) exhibited relatively low strength up to 1075 °C (16.94 MPa) because its low flux content delayed vitrification and densification, requiring higher firing temperatures to achieve adequate bonding. Only at 1150 °C did the MOR rise significantly to 63.72 MPa, as sufficient liquid phase finally formed to enhance particle bonding, eliminate pores, and improve microstructural integrity. This enhancement corresponds to the completion of sintering processes, increased bulk density, and the formation of a continuous microstructure with improved load-bearing capacity. All slag-containing compositions demonstrated superior mechanical performance compared to the control at equivalent temperatures. Among these, Sample 4 achieved an exceptional strength of 64.29 MPa at 1060 °C, significantly exceeding industry standards for both wall and floor applications. This enhancement is attributed to improved microstructural integrity, higher density, optimized particle packing, and the formation of strengthening crystalline phases facilitated by the fluxing action of slag components. The strength reduction observed above 1060 °C in slag samples correlates with the deterioration of physical properties and is attributed to increased MnO activity, elevated surface tension and viscosity, and thermal degradation effects, including grain growth and recrystallization [48].

Translucency measurements (Figure 10(b)) provide valuable insights into surface vitrification, optical properties, and self-glazing effectiveness, evaluated according to ASTM D523. These

measurements quantify surface gloss and light transmission as indicators of surface quality and microstructural densification [49].

The control composition showed progressive translucency enhancement with temperature, reaching 5.81% at 1150 °C, indicating gradual surface densification and glassy phase formation. Self-glazing for this composition initiated around 1100 °C, reaching maximum effectiveness at 1150 °C. The subsequent slight decrease in translucency is associated with stress relaxation and microstructural coarsening, potentially leading to microcrack formation or devitrification that disrupts light transmission. Remarkably, slag-containing samples demonstrated significantly enhanced translucency with an early onset around 1040 °C and peak values at 1060 °C. Sample 4 achieved exceptional translucency of 17.6%, representing a three-fold improvement over the control. This superior optical performance is attributed to the formation of a homogeneous glassy surface layer, promoted by the high concentration of fluxing oxides in the slag composition [22,23].

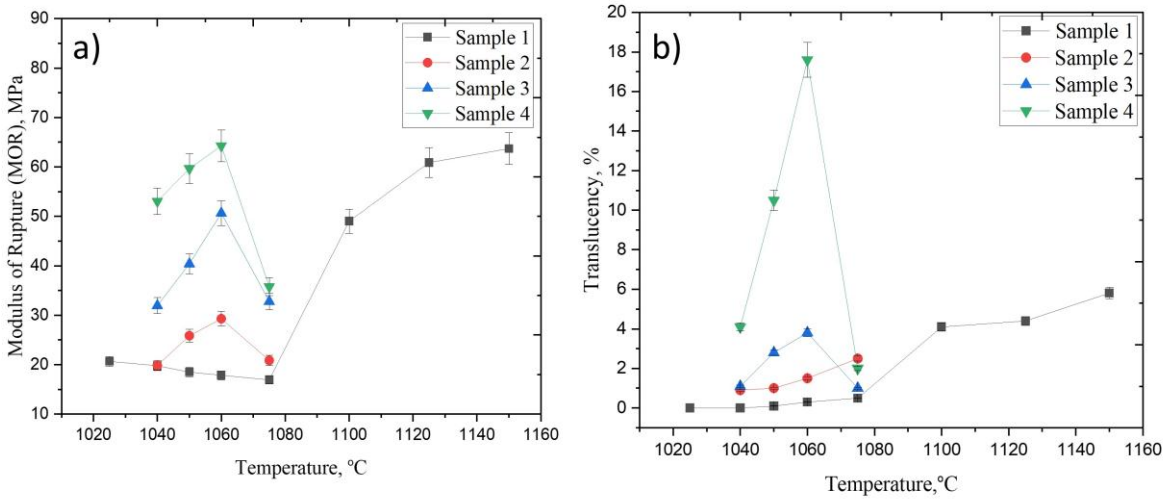


Figure 10: Modulus of rupture (MOR) test result and translucency results

These transition metal oxides effectively reduce the eutectic temperature of the system, facilitating early-stage vitrification and creating a smooth, reflective surface that enhances light transmission. The optimal self-glazing effect occurs at 1060 °C for Sample 4, producing tiles with excellent gloss, brightness, and aesthetic appeal while maintaining superior mechanical properties. The pronounced translucency is closely linked to the increased formation of a continuous glassy phase, which not only enhances optical properties but also contributes to surface compactness and improved durability. The resulting tiles exhibit excellent surface uniformity, enhanced brightness, and superior aesthetic appeal, confirming the significant role of IF slag as a functional additive in tailoring both mechanical and optical properties of self-glazed ceramic tiles [23,27].

Figure 11 depicts the visual appearance of fired ceramic samples (Samples 1–4) at various firing temperatures, showing progressive changes in coloration, surface reflectivity, and gloss with increasing temperature and IF slag content. Progressive darkening from light beige (1025–1060 °C) to deeper beige at higher temperatures, with smoothness and gloss developing only near 1150 °C. This indicates delayed vitrification and glass phase formation, which correlates

with thermodynamic predictions. In Sample 2, the vitrification temperature is reduced significantly with the addition of IF slag. Earlier color darkening (1040–1060 °C) to medium brown with moderate reflectivity is observed, with the surface becoming darker and smoother by 1075 °C, indicating improved vitrification onset. In Sample 3, a dark gray color develops at 1040–1050 °C, with clear surface gloss by 1060 °C. At 1075 °C, over-vitrification leads to melting and bloating, reducing optical uniformity. In Sample 4, deep black and high gloss are already evident at 1040 °C. By 1060 °C, the surface achieves maximum reflectivity and uniformity, characteristic of self-glazing. Over-firing at 1075 °C results in bloating and surface irregularities. Overall, increasing slag content lowers the vitrification onset temperature, enhances gloss, and deepens coloration. Sample 4 achieves optimal optical quality at 1060 °C, but higher firing temperatures risk over-firing defects. Controlled slag addition balances aesthetic quality with mechanical performance [22,24].

Comparison between experimental tiles and standard commercial ceramic tiles is presented in Table 5.

Table 5: Comparison of experimental tiles vs. standard commercial ceramic tiles

Property	**Sample 1**	**Sample 2**	**Sample 3**	**Sample 4**	**Standard commercial ceramic tiles**
Linear thermal expansion coefficient	—	—	—	6.7×10^{-3} °C^{-1}	typical range: 3.64–10.6×10^{-3} °C^{-1}
Linear shrinkage	4.97%	3.19%	3.18%	1.87%	≤ 5% (maximum)
Apparent porosity	0.028%	2.847%	2.19%	0.074%	≤ 10% (maximum)
Water absorption	3.95%	0.084%	0.036%	0.0045%	≤ 7% (maximum)
Bulk density	3.76 g/cm³	2.95 g/cm³	3.05 g/cm³	3.95 g/cm³	2.5–6 g/cm³
Modulus of rupture	63.72 MPa	29.25 MPa	50.65 MPa	64.29 MPa	Floor tiles: ≥ 35 MPa Wall tiles: ≥ 25 MPa
Optimum sintering temperature	1150 °C	1060 °C	1060 °C	1060 °C	1150 °C
Translucency	5.81%	2.5%	3.8%	17.6%	—

In the case of the linear thermal expansion coefficient, sample 4 falls well within the standard commercial range. This indicates good thermal compatibility with conventional ceramic bodies and glazes, reducing the risk of thermal cracking or crazing during cooling. Regarding linear shrinkage, all samples satisfy the maximum acceptable shrinkage limit. Sample 1 is close to the upper limit, indicating higher densification during sintering. Sample 4 shows the lowest shrinkage, suggesting controlled densification and better dimensional stability. In the matter of apparent porosity, all samples are far below the maximum limit. Samples 1 and 4 exhibit extremely low porosity, indicating highly dense and well-sintered microstructures. Low porosity improves mechanical strength, chemical resistance, and durability. In regard to water absorption, all samples meet the requirement. Samples 2, 3, and especially Sample 4 exhibit ultra-low water absorption, characteristic of vitrified or porcelain-grade tiles. This indicates excellent densification and minimal open

porosity. On the subject of bulk density, all samples fall within the acceptable density range. Sample 4 shows the highest density, which correlates with the lowest porosity, the lowest water absorption and the highest mechanical strength. This confirms superior sintering efficiency. In the case of modulus of rupture, Samples 1, 3, and 4 exceed floor tile requirements. Sample 2 satisfies wall tile requirements but does not meet the floor tile standard. The high MOR values of Samples 1 and 4 are consistent with their high density and low porosity. Samples 2, 3, and 4 achieve optimal properties at a lower temperature (1060 °C). This is significant because lower energy consumption, reduced production cost, lower CO_2 emissions and shorter firing cycles. This represents a major industrial advantage. And sample 4 shows remarkably high translucency. High translucency is typically associated with very low porosity, high vitrification, fine and homogeneous microstructure and reduced light scattering at grain boundaries. This suggests that Sample 4 has a highly glassy and dense phase distribution.

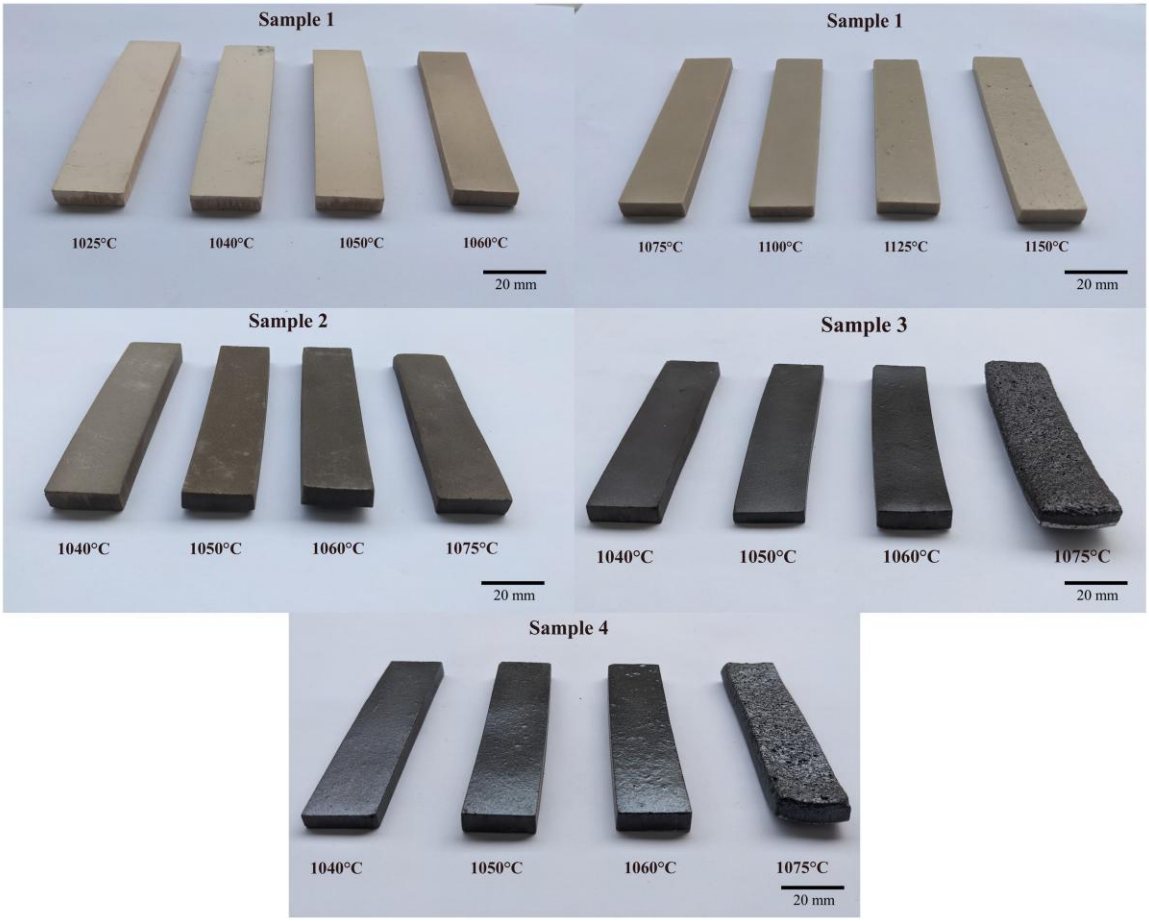


Figure 11: Visual analysis of the fired ceramic Sample 1 to Sample 4

4. Conclusion

This study investigated the sustainable production of self-glazed ceramic tiles using IF slag and waste glass as substitutes for conventional raw materials. Thermodynamic modeling with FactSage demonstrated that the incorporation of IF slag promoted early liquid-phase formation, enhanced fluxing behavior, and systematically reduced viscosity from about 10.9 log (Pa.s) at 900 °C to 6.5 log (Pa.s) at 1200 °C, with slag-rich compositions reaching as low as 3.6 log (Pa.s). These reductions brought melt viscosity into the optimal range of approximately 10^6–10^8 Pa.s, thereby lowering the firing temperature and reducing overall energy demand. Among

the evaluated systems, System 1 (clay-reduction strategy) exhibited superior vitrification and viscosity control, with Sample 4 (30 wt. % IF slag) providing the best industrially viable balance of performance and processing stability. XRD analysis further confirmed the elimination of mullite phases and progressive reduction of quartz peaks with increasing slag content, while the controlled formation of Mn-rich pyroxenoid phases such as rhodonite in Sample 4 offered a wider firing window and improved process stability. Experimental validation supported the modeling results, showing that slag-containing tiles achieved lower water absorption, reduced apparent porosity, and higher bulk density compared to the control composition. Mechanical strength was also significantly improved, with Sample 4 reaching a modulus of rupture of 64.29 MPa at 1060 °C, which exceeds ASTM requirements for both wall and floor tiles. In addition, optical and glazing properties were enhanced, as evidenced by early vitrification onset, increased surface gloss, and exceptional translucency (17.6%), producing high-quality self-glazed surfaces without the need for external glazing materials. Taken together, these findings confirm that the utilization of IF slag and waste glass not only reduces reliance on natural raw materials but also enables sustainable, energy-efficient ceramic tile production while contributing to waste valorization and circular economy practices.

5. Corresponding author:

Fahmida Gulshan;

Present Address: Faculty Member of Materials and Metallurgical Engineering, Bangladesh University of Engineering and Technology, Dhaka-1000, Bangladesh.

Phone: +8801733892419;

Email: fahmidagulshan@mme.buet.ac.bd

6. Declarations

Authorship contribution statement:

1. **S Sadakat Sharif:**

Writing– original draft, Writing– review & editing, Visualization, Software, Methodology, Investigation, Formal analysis, Data curation, Conceptualization.

2. **Rexona Khanom:**

Writing– original draft, Writing– review & editing, Visualization, Software, Methodology, Investigation, Formal analysis, Data curation, Conceptualization.

3. **Sazzad Ahmad:**

Writing Critical review & editing, Software, Investigation, Formal analysis, Data curation, Conceptualization.

4. **Bima Satritama:**

Writing– review & editing, Visualization, Software, Formal analysis, Data curation.

5. **M Akbar Rhamdhani:**

Writing– Critical review & editing, Software, Resources, Data curation.

6. **Muzahidur Rahman Chowdhury**

Writing– review & editing.

7. **Wahidur Rahman Sajal**

Writing– review & editing.

8. **Muhammad Hasanuzzaman:**

Writing– Critical review & editing, Resources, Investigation, Formal analysis, Data curation, Conceptualization.

9. **Fahmida Gulshan:**

Writing– Critical review & editing, Supervision, Resources, Investigation, Formal analysis, Data curation, Conceptualization, Fund acquisition, Project administration.

7. Funding information

This research received support from the Committee for Advanced Studies and Research (CASR), Bangladesh University of Engineering and Technology, for research activities only. The funding did not include any allocation for article processing charges, publication fees, or open-access costs. I do not have access to any other institutional, project, or external funding to cover the APC, and I am unable to pay the charge personally.

Declaration of Competing Interest:

The authors declare no competing interests or relationships influencing their work reported in this paper.

Declaration of generative AI and AI-assisted technologies in the manuscript preparation process:

During the preparation of this work, the author(s) did not use generative AI or AI-assisted technologies in any part of the manuscript writing, analysis, or editing process. All content was fully written, reviewed, and verified by the author(s), who take complete responsibility for its originality and accuracy.

8. Data Availability

The datasets used and analyzed during this study are available from the corresponding author on reasonable request.

9. References

1. Das, B.; Prakash, S.; Reddy, P.S.R.; Misra, V.N. An Overview of Utilization of Slag and Sludge from Steel Industries. *Resour. Conserv. Recycl.* **2007**, *50*, 40–57, doi:10.1016/j.resconrec.2006.05.008.
2. Motz, H.; Geiseler, J. Products of Steel Slags an Opportunity to Save Natural Resources. *Waste Manag.* **2001**, *21*, 285–293, doi:10.1016/s0956-053x(00)00102-1.
3. Piatak, N.M.; Parsons, M.B.; Seal, R.R. Characteristics and Environmental Aspects of Slag: A Review. *Appl. Geochem.* **2015**, *57*, 236–266, doi:10.1016/j.apgeochem.2014.04.009.

4. Huang, Y.; Bird, R.N.; Heidrich, O. A Review of the Use of Recycled Solid Waste Materials in Asphalt Pavements. *Resour. Conserv. Recycl.* **2007**, *52*, 58–73, doi:10.1016/j.resconrec.2007.02.002.
5. Rahman, M.S.; Barua, B.S.; Karim, M.R.; Kamal, M. Investigation of Heavy Metals and Radionuclide's Impact on Environment Due to the Waste Products of Different Iron Processing Industries in Chittagong, Bangladesh. *J. Environ. Prot.* **2017**, *8*, 974–989.
6. Ahmad, S.I.; Rahman, Md.S. Mechanical and Durability Properties of Induction-Furnace-Slag-Incorporated Recycled Aggregate Concrete. *Adv. Civ. Eng.* **2018**, *2018*, doi:10.1155/2018/3297342.
7. Baalamurugan, J.; Ganesh Kumar, V.; Naveen Prasad, B.S.N.; Padmapriya, R.; Karthick, V.; Govindaraju, K. Recycling of Induction Furnace Steel Slag in Concrete for Marine Environmental Applications towards Ocean Acidification Studies. *Int. J. Environ. Sci. Technol.* **2022**, *19*, 5039–5048, doi:10.1007/s13762-021-03362-7.
8. Ali, Z.H.; Khalid, N.N. Applicability of Induction Furnace Steel Slag in RC Columns Subjected to Axial and Uniaxial Loading. *Civ. Environ. Eng.* **2023**, *19*, 108–118, doi:10.2478/cee-2023-0010.
9. Birgonda, S.; Senthilkumar, R.; Ramesh, S.T. Induction Furnace Slag as Fine and Coarse Aggregate in Quaternary Blended Self-Compacting Concrete: A Comprehensive Study on Durability and Performance. *Mater. Today Sustain.* **2024**, *27*, 100873, doi:10.1016/j.mtsust.2024.100873.
10. Adegoke, H.A.; Ikumapayi, C.M. Effects of Induction Furnace Slag on the Durability Properties of Concrete. *Constr. Build. Mater.* **2024**, *419*, 135263, doi:10.1016/j.conbuildmat.2024.135263.
11. Baalamurugan, J.; Ganesh Kumar, V.; Chandrasekaran, S.; Balasundar, S.; Venkatraman, B.; Padmapriya, R.; Bupesh Raja, V.K. Utilization of Induction Furnace Steel Slag in Concrete as Coarse Aggregate for Gamma Radiation Shielding. *J. Hazard. Mater.* **2019**, *369*, 561–568, doi:10.1016/j.jhazmat.2019.02.064.
12. Baalamurugan, J.; Ganesh Kumar, V.; Stalin Dhas, T.; Taran, S.; Nalini, S.; Karthick, V.; Ravi, M.; Govindaraju, K. Utilization of Induction Furnace Steel Slag Based Iron Oxide Nanocomposites for Antibacterial Studies. *SN Appl. Sci.* **2021**, *3*, doi:10.1007/s42452-021-04299-9.
13. Da Costa Avelar, T.; De Souza, R.M.; Durante, T.; Grillo, F.F.; Vieira, E.A.; Junca, E.; De Paola, J.C.C.; De Oliveira, J.R. Influence of Physicochemical Properties and Chemical Composition of Slags on the Slag Foaming Index. *JOM* **2023**, *75*, 2045–2053, doi:10.1007/s11837-022-05685-3.
14. Regordosa, A.; Llorca-Isern, N. Chemical and Structural Characterization of Slag Compounds Formed in the Melting Processes to Produce Spheroidal Graphite Cast Irons. *Int. J. Met.* **2016**, *10*, 421–434, doi:10.1007/s40962-016-0025-7.
15. Fu, S.; Lee, J. Recycling of Ceramic Tile Waste into Construction Materials. *Dev. Built Environ.* **2024**, *18*, 100431, doi:10.1016/j.dibe.2024.100431.
16. Souza, G.P.; Rambaldi, E.; Tucci, A.; Esposito, L.; Lee, W.E. Microstructural Variation in Porcelain Stoneware as a Function of Flux System. *J. Am. Ceram. Soc.* **2004**, *87*, 1959–1966, doi:10.1111/j.1151-2916.2004.tb06347.x.
17. Nodehi, M.; Mohamad Taghvaee, V. Sustainable Concrete for Circular Economy: A Review on Use of Waste Glass. *Glass Struct. Eng.* **2022**, *7*, 3–22, doi:10.1007/s40940-021-00155-9.
18. Hamada, H.; Alattar, A.; Tayeh, B.; Yahaya, F.; Thomas, B. Effect of Recycled Waste Glass on the Properties of High-Performance Concrete: A Critical Review. *Case Stud. Constr. Mater.* **2022**, *17*, e01149, doi:10.1016/j.cscm.2022.e01149.

19. Qaidi, S.; Najm, H.M.; Abed, S.M.; Özkılıç, Y.O.; Al Dughaishi, H.; Alosta, M.; Sabri, M.M.S.; Alkhatib, F.; Milad, A. Concrete Containing Waste Glass as an Environmentally Friendly Aggregate: A Review on Fresh and Mechanical Characteristics. *Materials* **2022**, *15*, 6222, doi:10.3390/ma15186222.
20. Khan, Md.N.N.; Saha, A.K.; Sarker, P.K. Reuse of Waste Glass as a Supplementary Binder and Aggregate for Sustainable Cement-Based Construction Materials: A Review. *J. Build. Eng.* **2020**, *28*, 101052, doi:10.1016/j.jobe.2019.101052.
21. De Faria Busch, P.; Marvila, M.T.; Girondi Delaqua, G.C.; Vieira, C.M.F. Recycling of Waste Glass Extracted from a WTP into Ceramic Materials. *J. Mater. Cycles Waste Manag.* **2022**, *24*, 763–774, doi:10.1007/s10163-022-01358-0.
22. Delaqua, G.; Magalhães, J.; Marvila, M.; Vernilli, F.; Monteiro, S.; Colorado, H.; Vieira, C. Application of Glass Waste on Red Ceramic to Improve Sintering. *Sustainability* **2022**, *14*, 10454, doi:10.3390/su141610454.
23. Lemougna, P.N.; Yliniemi, J.; Nguyen, H.; Adesanya, E.; Tanskanen, P.; Kinnunen, P.; Roning, J.; Illikainen, M. Utilisation of Glass Wool Waste and Mine Tailings in High Performance Building Ceramics. *J. Build. Eng.* **2020**, *31*, 101383, doi:10.1016/j.jobe.2020.101383.
24. Huang, Y.; Chen, Z.; Liu, Y.; Lu, J.-X.; Bian, Z.; Yio, M.; Cheeseman, C.; Wang, F.; Sun Poon, C. Recycling of Waste Glass and Incinerated Sewage Sludge Ash in Glass-Ceramics. *Waste Manag.* **2024**, *174*, 229–239, doi:10.1016/j.wasman.2023.12.007.
25. Liu, B.; Yang, Q.-W.; Zhang, S.-G. Integrated Utilization of Municipal Solid Waste Incineration Fly Ash and Bottom Ash for Preparation of Foam Glass–Ceramics. *Rare Met.* **2019**, *38*, 914–921, doi:10.1007/s12598-019-01314-2.
26. Zhang, J.; Liu, B.; Zhang, S. A Review of Glass Ceramic Foams Prepared from Solid Wastes: Processing, Heavy-Metal Solidification and Volatilization, Applications. *Sci. Total Environ.* **2021**, *781*, 146727, doi:10.1016/j.scitotenv.2021.146727.
27. Zou, W.; Zhang, W.; Pi, Y.; Zhang, Y.; Chen, Y.; Zhang, L. Study on Preparation of Glass-Ceramics from Multiple Solid Waste and Coupling Mechanism of Heavy Metals. *Ceram. Int.* **2022**, *48*, 36166–36177, doi:10.1016/j.ceramint.2022.08.173.
28. Sarkar, R.; Singh, N.; Das Kumar, S. Utilization of Steel Melting Electric Arc Furnace Slag for Development of Vitreous Ceramic Tiles. *Bull. Mater. Sci.* **2010**, *33*, 293–298, doi:10.1007/s12034-010-0045-5.
29. Teo, P.-T.; Anasyida, A.S.; Basu, P.; Nurulakmal, M.S. Recycling of Malaysia's Electric Arc Furnace (EAF) Slag Waste into Heavy-Duty Green Ceramic Tile. *Waste Manag.* **2014**, *34*, 2697–2708.
30. Furlani, E.; Tonello, G.; Maschio, S. Recycling of Steel Slag and Glass Cullet from Energy Saving Lamps by Fast Firing Production of Ceramics. *Waste Manag.* **2010**, *30*, 1714–1719.
31. Zhao, L.; Li, Y.; Zhou, Y.; Cang, D. Preparation of Novel Ceramics with High CaO Content from Steel Slag. *Mater. Des.* **2014**, *64*, 608–613.
32. Ghosh, S.; Das, M.; Chakrabarti, S.; Ghatak, S. Development of Ceramic Tiles from Common Clay and Blast Furnace Slag. *Ceram. Int.* **2002**, *28*, 393–400.
33. Ozturk, Z.B.; Gultekin, E.E. Preparation of Ceramic Wall Tiling Derived from Blast Furnace Slag. *Ceram. Int.* **2015**, *41*, 12020–12026.
34. Baccarin, L.I.P.; Bragança, S.R. Thermodynamic Simulations for Optimizing the Firing of Traditional Ceramic Formulations Using Waste Glass as a Flux. *Mater. Today Commun.* **2024**, *38*, 107913, doi:10.1016/j.mtcomm.2023.107913.
35. Suvaci, E.; Tamsu, N. The Role of Viscosity on Microstructure Development and Stain Resistance in Porcelain Stoneware Tiles. *J. Eur. Ceram. Soc.* **2010**, *30*, 3071–3077, doi:10.1016/j.jeurceramsoc.2010.06.010.

36. Bene, P.; Bardaro, D.; Bello, D.; Manni, O. Numerical Modeling and Experimental Characterization of the Pyroplasticity in Ceramic Materials during Sintering.; October 27 2010; pp. 203–208.
37. Baccarin, L.I.P.; Bielefeldt, W.V.; Bragança, S.R. Prediction of Glass Phase Viscosity in Firing Traditional Ceramics and Porcelain Tiles with Waste Glass Powder. *Open Ceram.* **2023**, *15*, 100417, doi:10.1016/j.oceram.2023.100417.
38. Neuville, D.R. Viscosity, Structure and Mixing in (Ca, Na) Silicate Melts. *Chem. Geol.* **2006**, *229*, 28–41, doi:10.1016/j.chemgeo.2006.01.008.
39. Khater, G.A.; Nabawy, B.S.; El-Kheshen, A.A.; Abdel Latif, M.A.-B.; Farag, M.M. Use of Arc Furnace Slag and Ceramic Sludge for the Production of Lightweight and Highly Porous Ceramic Materials. *Materials* **2022**, *15*, 1112, doi:10.3390/ma15031112.
40. Pal, M.; Das, S.; Gupta, S.; Das, S.K. Thermal Analysis and Vitrification Behavior of Slag Containing Porcelain Stoneware Body. *J. Therm. Anal. Calorim.* **2016**, *124*, 1169–1177, doi:10.1007/s10973-015-5179-7.
41. Gao, Z.; Iii, C.H.D. Thermal Analysis of Nucleation and Growth of Crystalline Phases in Vitrified Industrial Wastes. *J. Am. Ceram. Soc.* **1999**, *82*, 561–565, doi:10.1111/j.1151-2916.1999.tb01801.x.
42. Zhu, Y.; Yu, X.; Pan, S.; Nong, P.; Kong, Q.; Wang, X.; Zhang, L.; Tan, S.; Zhu, Z. Dissolution of the Smithsonite–Rhodochrosite (ZnCO3-MnCO3) Solid Solutions in Aqueous Solution at 25 °C. *Chem. Geol.* **2022**, *602*, 120886, doi:10.1016/j.chemgeo.2022.120886.
43. Meena, R.; Mallik, M.; Yadav, R.; Meena, A.; Hashmi, A.W. Investigation of Physical Properties of Bamboo Dust with Marble Powder Filled Ceramic Composites: Sustainable Approach for Ceramic Tiles Manufacturing. *Proc. Inst. Mech. Eng. Part J. Mater. Des. Appl.* **2024**, *238*, 1425–1437, doi:10.1177/14644207231225067.
44. Ozdemir, I.; Yilmaz, S. Processing of Unglazed Ceramic Tiles from Blast Furnace Slag. *J. Mater. Process. Technol.* **2007**, *183*, 13–17, doi:10.1016/j.jmatprotec.2006.09.002.
45. Mostafa, N.Y.; Shaltout, A.A.; Abdel-Aal, M.S.; El-maghraby, A. Sintering Mechanism of Blast Furnace Slag–Kaolin Ceramics. *Mater. Des.* **2010**, *31*, 3677–3682, doi:10.1016/j.matdes.2010.03.001.
46. Abed, G.A.; Manii, J.K.; Ali, J.H. Some Engineering Properties of Ancient Fire Clay Bricks Discovered at the Dilbat Archaeological Site, South of Hilla City. *Iraqi Geol. J.* **2022**, 121–130, doi:10.46717/igj.55.1B.12Ms-2022-02-28.
47. Melchiades, F.G.; Rego, B.T.; Higa, S.M.; Alves, H.J.; Boschi, A.O. Factors Affecting Glaze Transparency of Ceramic Tiles Manufactured by the Single Firing Technique. *J. Eur. Ceram. Soc.* **2010**, *30*, 2443–2449, doi:10.1016/j.jeurceramsoc.2010.04.030.
48. Conte, S.; Fantini, R.; Arletti, R.; Molinari, C.; Dondi, M.; Zanelli, C.; Gualtieri, A.F. Sintering Mechanisms, Phase Transformations and Microstructure of Porcelain Stoneware Containing Thermally Inertized Man-Made Vitreous Fibres. *J. Eur. Ceram. Soc.* **2025**, *45*, 117230, doi:10.1016/j.jeurceramsoc.2025.117230.
49. Manziuc, M.; Gasparik, C.; Burde, A.V.; Colosi, H.A.; Negucioiu, M.; Dudea, D. Effect of Glazing on Translucency, Color, and Surface Roughness of Monolithic Zirconia Materials. *J. Esthet. Restor. Dent.* **2019**, *31*, 478–485, doi:10.1111/jerd.12493.